Effects of the Glycocalyx on the Electrophoretic Mobility of Red Cells and on Streaming Potentials in Blood Vessels: Predictions of a Structurally-Based Model

By A. J. MESTEL[1], A. J. MOKADY[1,2], K. H. PARKER[2] AND C. P. WINLOVE[2]

[1]Mathematics Department, Imperial College, 180 Queen's Gate, London SW7 2BZ, UK.

[2]Centre for Biological and Medical Systems, Imperial College, London SW7 2AZ, UK.

Correspondence to A. J. Mestel as above; e-mail a.j.mestel@ic.ac.uk

(Received September 1998 and in revised form February 1999)

The polyelectrolyte layer coating mammalian cells, known as the glycocalyx, may be important in communicating flow information to the cell. In this paper, the layer is modelled as a semi-infinite, doubly periodic array of parallel charged cylinders. The electric potential and ion distributions surrounding such an array are found using the linearised Poisson-Boltzmann equation and an iterative domain decomposition technique. Similar methods are used to calculate Stokes flows, driven either by a shear at infinity or by an electric field, parallel or transverse to the cylinders. The resulting electric streaming currents due to flow over endothelial cells, and the electrophoretic mobilities of red blood cells are deduced as functions of polymer concentration and electrolyte molarity. It is shown that only the top portion of the layer is important in these effects.

Introduction

The plasma membranes of erythrocytes and endothelial cells are covered with a layer of membrane-bound glycoproteins and plasma proteins, known as the glycocalyx. The glycocalyx is highly charged and its interactions with moving electrolyte generate various electrokinetic effects. For example, the flow of blood across the endothelial surface generates streaming currents and potentials. Arguing by analogy with electrokinetic phenomena in connective tissues such as cartilage and bone, it has been suggested that these may be important in transducing information about blood flow to the underlying tissue. As another example, electrical interactions between blood cells are important to many aspects of haemorheology. The mobility of red cells in an electric field has also been extensively investigated, both as a means of probing the structure of the glycocalyx and as an indicator of haemorheological abnormalities.

A number of structurally based theoretical models of the electrokinetic phenomena generated by flow through extracellular matrix have been developed (e.g. Buschmann & Grodzinsky 1995, Chammas *et al.* 1994 Eisenberg & Grodzinsky 1988). The effects of flow over polylelectrolyte layers has received less attention (Weinbaum 1998). The majority of investigators have used a continuum approach which has made it difficult to relate the predictions to the molecular structure and organisation of the glycocalyx.

In order to overcome this difficulty we have recently developed a model in which the glycoproteins are represented as an array of charged rods (Mokady, Mestel & Winlove (1998), henceforth referred to as MMW). We used the approach of Larson and Higdon (1986 & 1987) to calculate flow at different depths in the array resulting from a shear flow across the surface or from an imposed electric field. Ion distributions were calculated using a geometrically consistent version of Katchalsky's (1971) rod-in-cell model of polyelectrolytes. The resulting streaming currents and potentials were calculated for a number of representative situations.

The aims of the present work are to summarise the physiologically relevant conclusions and to compare the theoretical predictions with published data on red cell electrophoresis and streaming potentials in blood vessels. In addition, we determined the sensitivity of the theory to choice of parameters and experimental conditions. We also point out certain predictions of the theory which have implications for the design of future experiments.

A preliminary report on this work was given at the 2nd International Conference on Multiphase Flow, Kyoto, 1995, while details of the computational method are given in (MMW).

Theoretical Model

Electrical Potential and Ion Distributions

Since the model has been described in detail elsewhere (MMW), we shall only outline its physical basis and summarise the principal results in the following section. Except where explicitly stated, all variables are in SI units. The glycoproteins of the glycocalyx are modelled as cylindrical rods of radius a with a uniform surface charge density arranged in a square array (Figure 1).

The potential field, Φ, around each cylinder satisfies the Poisson equation:

$$\nabla^2\Phi = -\frac{\rho}{\varepsilon} \tag{2.1}$$

where ε is the constant permittivity of the solution. Each of the I distinct ion species is assumed to satisfy a Boltzmann distribution, so that the charge density, ρ is given by:

$$\rho(\Phi) = \sum_{i=1}^{I} e z_i n_i^0 \exp\left(-\frac{e z_i}{kT}\Phi\right) \ , \tag{2.2}$$

where $-e$ is the charge of an electron, k is Boltzmann's constant, T is the absolute temperature, while n_i^0 is the concentration infinitely far from the rods and z_i the valency of ion type i. For small potentials ($\phi \equiv e\Phi/kT \ll 1$) equations (2.1) and (2.2) may be linearised. Electrical neutrality far from the glycocalyx requires $\sum z_i n_i^0 = 0$, and so

$$\rho = -\varepsilon\kappa^2\Phi \qquad \text{and} \quad \nabla^2\Phi = \kappa^2\Phi \tag{2.3}$$

where κ^{-1} is the Debye length, given by

$$\kappa^2 = \frac{e^2}{\varepsilon kT}\sum_{i=1}^{I} z_i^2 n_i^0 \ . \tag{2.4}$$

On the cylinders, the boundary condition

$$\frac{\partial \Phi}{\partial r} = q \qquad \text{on} \quad r = a \tag{2.5}$$

is imposed, corresponding to a charge density per unit axial length $-2\pi a \varepsilon q$ C/m.

For an isolated cylinder, (2.3) with (2.5) has the solution

$$\Phi = \frac{q}{\kappa} \frac{K_0(\kappa r)}{K_0'(\kappa a)} \ , \tag{2.6}$$

where K_n and below, I_n, denote modified Bessel functions of order n. The $'$ denotes differentiation with respect to the argument, and $K_0' < 0$. Note that the solution (2.6) is equivalent to the potential of mobile ions around a line charge of strength σ_0 at $r = 0$, where

$$\sigma_0 = \frac{2\pi\varepsilon q}{\kappa K_0'(\kappa a)} \ . \tag{2.7}$$

Consider first a doubly periodic array of cylinders with separation $2b$, so that the potential is the same within each square domain. Then within each square Φ is determined by (2.4) with (2.5) and the symmetry conditions

$$\frac{\partial \Phi}{\partial x} = 0 \qquad \text{on} \quad |x| = b \qquad \text{and} \quad \frac{\partial \Phi}{\partial y} = 0 \qquad \text{on} \quad |y| = b \ . \tag{2.8}$$

A simple approximation to the potential can be obtained by replacing each charged cylinder with a line charge of strength (2.7) at its centre. This gives the result

$$\Phi(\mathbf{r}) = \frac{\sigma_0}{2\pi\varepsilon} \sum_{m,n} K_0 \Big[\kappa \big| \mathbf{r} - 2b(m\mathbf{i} + n\mathbf{j}) \big| \Big] \tag{2.9}$$

where $\mathbf{i}$ and $\mathbf{j}$ are unit vectors in the x and y-directions respectively. This approximation is easy to use in a variety of configurations and deserves wider application.

An alternative "cylindrical cell" approximation was proposed by Katchalsky (1971), in which the outer boundary of each square cell is replaced by a cylindrical boundary of radius $b_0 = 2b/\sqrt{\pi}$ chosen so that the solid volume fraction is the same as in the true geometry. Imposing the condition $\Phi'(b_0) = 0$ gives

$$\Phi(r) = \frac{q}{\kappa} \left(\frac{I_0'(\kappa b_0) K_0(\kappa r) - K_0'(\kappa b_0) I_0(\kappa r)}{K_0'(\kappa a) I_0'(\kappa b_0) - I_0'(\kappa a) K_0'(\kappa b_0)} \right) \ . \tag{2.10}$$

The exact solution to (2.3), (2.5) and (2.8) can be expressed as a Fourier series. Imposing only the boundary condition (2.5),

$$\Phi(r, \theta) = q \, \frac{K_0(\kappa r)}{\kappa K_0'(\kappa a)} + qa \sum_{n=0}^{\infty} a_n \left(\frac{I_n(\kappa r)}{I_n'(\kappa a)} - \frac{K_n(\kappa r)}{K_n'(\kappa a)} \right) \cos n\theta \ . \tag{2.11}$$

The unknown coefficients a_n are determined by the boundary conditions (2.8). Truncating the infinite series after N terms, and applying (2.8) at M sampled points on the boundary, where $M > N$, results in an over-determined system of linear algebraic equations for the coefficients. Due to the eightfold symmetry $a_n \neq 0$ only if $n = 4m$ and only points in $0 < \theta < \frac{1}{4}\pi$ need to be sampled. Numerical solutions were found using the LAPACK linear least-squares solver "*dgels*".

We showed in (MMW) that for a charge density which varies periodically along the cylinder axis:

$$q = q_0 + q_1 \cos \alpha z \tag{2.12}$$

the potential may be written as a sum of two components:

$$\Phi = \Phi_0(r,\,\theta) + \Phi_1(r,\,\theta)\cos\alpha z \tag{2.13}$$

where Φ_1 satisfies (2.3) with κ replaced by an effective Debye length β given by $\beta^2 = \alpha^2 + \kappa^2$. The exponential decay rate of Φ_1 is therefore greater than that of Φ_0, so that at fairly short distances from the cylinder the potential Φ is dominated by the z-independent component. Any experimentally measurable properties, such as osmotic pressure, which depend on the potential at some distance from the molecule, will thus depend only on Φ_0, and will not be affected by the microscopic variation along the molecule. This argument can be generalised to any periodic charge distribution and therefore helps to justify the use of a uniformly-charged cylinder as a model for a molecule consisting of point charges.

In MMW, the glycocalyx was modelled as a semi-infinite array, so that there were no cylinders in $x > 0$. The potential then varied between successive square domains, and the boundary conditions at $x = \pm b$ were replaced by continuity requirements. Within each domain expansions similar to (2.11) were used, but the reduced symmetry requires more coefficients a_n. For $x > 0$, the potential can be written

$$\Phi = qa\sum_{n=0}^{\infty}\gamma_n \exp\left(-\left(\kappa^2 + \frac{n^2\pi^2}{b^2}\right)^{1/2}x\right)\cos\frac{n\pi y}{b}\ , \tag{2.14}$$

for unknown coefficients γ_n. The resulting set of equations was solved iteratively, solving initially for the top layer of cells and using the solution in one layer of cells to determine approximate boundary conditions for the underlying layer. In each cell, at each iteration, the unknown coefficients were found by least squares methods as before. The procedure allowed the surface charge to vary between layers.

Flow Fields

Because of linearity, flow through the glycocalyx can be regarded as the superposition of two components, an axial flow parallel to the cylinders and a transverse flow perpendicular to them. Flow across the endothelial cell glycocalyx is driven by the macroscopic pressure gradient in the vessel but, on the length scale of the glycocalyx, its effect can be represented totally by a shear flow at infinity. In electrophoresis the flow is driven by the applied electric field. In either case, the electrical force caused by local variation in the electric potential, $\rho(\Phi)\nabla\Phi$, is conservative. It is therefore balanced by a local pressure gradient and has no effect on the velocity to leading order. The fluid velocity does, however, give rise to a streaming current or potential as calculated below.

For axial flow, with no imposed electric field or axial pressure gradient, the Stokes equations for the unidirectional velocity $\mathbf{u} = (0,\,0,\,u(x,\,y))$ reduce to:

$$\nabla^2 u = 0\ . \tag{2.15}$$

For flow driven by a shear of magnitude λ above the layer the boundary conditions are:

$$\frac{\partial u}{\partial x} \to \lambda \qquad \text{as} \quad x \to \infty \qquad \text{and} \quad u \to 0 \qquad \text{as} \quad x \to -\infty\ , \tag{2.16}$$

while no-slip on the cylinders and the periodicity in the y-direction require

$$u = 0 \qquad \text{on} \quad r_i = a, \qquad \frac{\partial u}{\partial y} = 0 \qquad \text{on} \quad y = \pm b\ . \tag{2.17}$$

Here $(r_i,\,\theta_i)$ denote polar coordinates centred on the i^{th} cylinder. This problem is solved

by a domain decomposition method similar to that used in the electrical potential calculations. The velocity is expanded

$$u(r_i, \theta_i) = \zeta_{i0} \ln r_i + \sum_{n=1}^{\infty} \zeta_{in} (r_i^n - r_i^{-n}) \; cosn\theta_i \; . \tag{2.18}$$

in each square subdomain and

$$u(x, y) = \eta_0 + \lambda x + \sum_{n=1}^{\infty} \eta_n \exp\left(-\frac{n\pi x}{b}\right) \cos\left(\frac{n\pi y}{b}\right) \; . \tag{2.19}$$

above the layer. The constants ζ_{in} and η_n are found numerically.

For the transverse flow, the velocity can be represented by a streamfunction $\Psi(x, y)$, so that $\mathbf{u} = (\Psi_y, -\Psi_x, 0)$ and the Stokes equations become:

$$\nabla^2 \Psi = -\omega, \qquad \nabla^2 \omega = 0 \; . \tag{2.20}$$

The expansions and solution procedure are more lengthy in this case and are given in MMW.

Calculation of Streaming Current

Flow parallel to the cylinders advects ions giving rise to a current density $j(x, y) = \rho u$. The total streaming current per unit glycocalyx length is given by

$$J = \frac{1}{2b} \int_{-b}^{b} \int_{-\infty}^{\infty} \rho u \, dx \, dy = -\frac{\varepsilon \kappa^2}{b} \int_{0}^{b} \int_{-\infty}^{\infty} u\Phi \, dx \, dy \; . \tag{2.21}$$

Such axial flow does not disturb the ion distribution. However, similar advection by flow perpendicular to the cylinders would alter the ion density ρ, and as discussed in MMW, it is necessary to include a term due to Brownian motion instantaneously restoring electrical equilibrium. Even with this term included, the net streaming current is notably smaller for transverse rather than axial flow, for hydrodynamical reasons.

Calculation of Electrophoretic Mobility

When a field $(0, 0, E)$ is applied parallel to the cylinders and cell surface, the fluid velocity satisfies:

$$\mu \nabla^2 u = -\rho E = \kappa^2 \varepsilon E \Phi \; , \tag{2.22}$$

where μ is the viscosity. Using (2.3), a particular solution to (2.22) is $u = \varepsilon E \Phi / \mu$, to which expansions of the form (2.16) and (2.17) must be added. When the field is parallel to the cell surface but perpendicular to the rods, the governing equations become:

$$\nabla^2 \Psi = -\omega, \qquad \nabla^2 \omega = \kappa^2 \frac{\varepsilon E}{\mu} \frac{\partial \Phi}{\partial x} \; . \tag{2.23}$$

In each case the potential Φ is as calculated above. Both equations are solved numerically in MMW using the methods outlined above.

Results

Choice of Parameters

Very little is known about the physico-chemical properties of the cell-surface polymers. Modelling them as uniformly charged cylinders introduces further arbitrariness into the choice of parameters. For the charge spacing except when specified otherwise, we shall take 1.6 nm, a value measured for heparan sulphate which is probably representative of the more highly charged components of the glycocalyx. For the rod radius we shall take $a = 0.5$ nm. This value is not inconsistent with structural data and has been shown to give a good fit between calculations of ion distributions and osmotic pressures calculated using a cylindrical cell model and a large body of experimental data on glycosaminoglycans and proteoglycans (e.g. Buschmann & Grodzinsky 1995). The concentration of polymer in the glycocalyx is not well-characterised. Estimates for endothelial cells suggest a concentration of 10% v/v, but this is believed to be an upper bound. We therefore present results for concentrations of 10% and 1% which should encompass the physiological range. The charge density for a 1% concentration is then $1.3 \times 10^6 C/m^3$. The final variable is the electrical permittivity of the solution. Permittivity is a function of salt concentration and a range of values are employed in molecular dynamics simulations, but in the absence of any consensus we shall use the value for pure water, $\varepsilon = 6.91 \times 10^{-10}$ C^2/(Jm).

Electrostatic Effects

Results are presented in terms of the non-dimensional potential $\phi = e\Phi/(kT)$. Figure 2 shows the effects of polymer concentration on the average potential at the outer boundary of the square domain. This potential is a determinant of many of the colligative properties of the polymer array. Note that over the concentration range estimated for cell-surface polymers (1% – 10%) the potential varies approximately 5-fold, though at higher polymer concentrations the sensitivity is reduced. A 10-fold reduction in ionic strength, as is often used experimentally to amplify electrokinetic effects, increases the potential by up to an order of magnitude. Unlike the cylindrical-cell model, the rod in square-cell model is space-filling, giving rise to a non-cylindrically symmetric potential field within the cell, as shown in Figure 3a. The figure also demonstrates that the solution for the cylindrical cell is close to the average value for the square cell.

Given the additional computational complexity of the square-cell model (2.11), it is pertinent to compare its predictions with the simpler cylindrical-cell (2.10) and line-charge (2.9) approximations. From Figure 3b it is apparent that over the physiological range of polymer concentrations both of the simpler models are close to the square-cell model, the line-charge model being almost indistinguishable. However, the line-charge approximation is incompatible with the fluid-flow coupling which is the thrust of the present work.

A widely used simplification is the linearisation of the Poisson-Boltzmann equation. The effect of this is shown in Figure 4 where the non-linear Poisson-Boltzmann equation has been solved for a monovalent electrolyte using a cylindrical cell approximation as in Winlove & Parker (1987). At a polymer concentration of 10%, the potentials are indistinguishable at physiological ionic strength, although they differ significantly at 0.015 M. However, at a polymer concentration of 1%, little difference is evident even at the lower salt concentrations.

The potential close to the surface of a polymer layer is shown in Figure 5 for two polymer concentrations at a low molarity both for the exact solution (2.11) with (2.14) and for the line-charge approximation. The most striking observation is that even under conditions of minimal shielding, high polymer concentration and low ionic strength (Figure 5a), the effect of the surface is apparent only in the first 2-3 layers of rods. In the solution phase the potential decays exponentially over the Debye length-scale. The line-charge approximation is very close to the more exact solution at low polymer concentrations (Figure 5b), but significant differences occur when the Debye length is comparable with the cylinder separation distance as in Figure 5a. In fact, for the unrealistically high potential values of Figure 5a, the linearisation of the Poisson-Boltzmann equation is also dubious.

The distributions of co- and counter-ions are shown in Figure 6 for a 0.15 M saline solution, for which the Debye length $\kappa^{-1} = 0.76$ nm. Physiologically the most pertinent observation is that the distribution within the glycocalyx is unaffected by the presence of the boundary except for the outermost layer of rods where the distribution decays on a scale determined by the Debye length. It should be noted that an additional effect of the glycocalyx is to cause a 2-fold imbalance in the numbers of anions and cations actually in contact with the plasma membrane, which might be important for the functioning of ion channels in the membrane. In the solution, the potential decays exponentially and the ion distribution is undisturbed beyond 3 nm. This demonstrates that electrical interactions between cells are likely to be important only when the distance of approach of the cells is less than 6 nm. However, whereas the electric potential decays exponentially outside the surface layer, hydrodynamic interactions between cells decay algebraically. Thus when cells are in close proximity, the induced streaming potentials may vary because of changes in the local shear rate, even when the ion concentrations do not.

One consequence of the asymmetry of the potential in the surface is the generation of a net force on the uppermost cylinders. We show in MMW that the magnitude of the electrostatic force per unit glycocalyx length is

$$F_i = \varepsilon q^2 a \pi \beta_{i1} \tag{3.1}$$

where

$$\beta_{im} = a_{im} \left(\frac{I_m(\kappa a)}{I'_m(\kappa a)} - \frac{K_m(\kappa a)}{K'_m(\kappa a)} \right) \quad , \tag{3.2}$$

where a_{im} are the Fourier coefficients in (2.11) calculated in the i^{th} domain. The electric forces on the ions are balanced by the gradient of a pressure, $p = \frac{1}{2}\kappa^2 \Phi^2 \varepsilon$, which gives rise to an osmotic pressure acting on the polymer. The net pressure force in the x-direction on the i^{th} cylinder per unit cylinder length is

$$G_i \simeq -\pi \kappa^2 a^3 \varepsilon q^2 \beta_{i1} \left(\frac{K_0(\kappa a)}{\kappa a K'_0(\kappa a)} + \beta_{i0} \right) \tag{3.3}$$

The total force per unit length acting on the ith cylinder is $F_i + G_i$. In most circumstances $F_i \gg G_i$, but in conditions of high shielding osmotic pressure can be the larger, though both forces are then small.

The electrostatic force can be thought of as the mutual repulsion of the incompletely screened cylinders from each other. The most significant contribution to the total force on the glycocalyx is due to the force on the topmost layer of cylinders due to the cylinders directly below them. In the high shielding limit, $\kappa b \to \infty$, this can be shown to be

$$F_0 \simeq \frac{\varepsilon q^2 a \pi^{3/2}}{\kappa^2 a^2 K'_0(\kappa a) K'_1(\kappa a)} \frac{e^{-2b\kappa}}{(b\kappa)^{1/2}} \quad . \tag{3.4}$$

	1%	5%	10%
0.015M	3.3×10^{-5}	6×10^{-4}	1.7×10^{-3}
0.15 M	3×10^{-8}	2×10^{-5}	1.2×10^{-4}
1.5 M	5.9×10^{-18}	2.5×10^{-9}	2.9×10^{-7}

TABLE 1. Force on uppermost cylinders per length of glycocalyx in N/m for varying ionic strengths and v/v polymer concentrations.

Table 1 shows the variation in force per unit length on the topmost cylinder at various polymer concentrations and ionic strengths. Under conditions of low shielding, the force is comparable to that necessary to elongate long polymer molecules. Thus if, as is expected, the polysaccharide chains of the glycocalyx are extremely flexible, this force may cause expansion of the glycocalyx or oppose its collapse under applied forces.

Streaming Currents

We show in MMW that shear flow over the surface of the glycocalyx either along the axis of the rods or perpendicular to them generates a velocity profile within the layer which decays to a self-similar form exponentially with depth below the surface. Increasing polymer concentration reduces fluid velocity and increases the rate of decay. Under physiological conditions it is probable that self-similarity is attained below the top one or two layers of the cylinders.

Above the cylinders, from (2.19) the velocity approaches exponentially the shear flow above a virtual plate positioned at $x = x^* \equiv -\eta_0/\lambda$ where λ is the shear rate far from the surface, so that $u \to \lambda(x - x^*)$ as $x \to \infty$. Thus the glycocalyx has the fluid mechanical effect of moving the apparent cell boundary to a position approximately one rod spacing below the surface of the glycocalyx. This may be particularly important in flow in the microvasculature (Damiano 1998). Clearly, however, flow effects are unlikely to be propagated as far as the plasma membrane itself, suggesting that components involved in the primary stages of flow transduction must be positioned in the glycocalyx rather than the cell membrane.

The local current density $j(x, y) = \rho u$ generated by axial flow is shown in Figure 7. It will be noted that, as expected from the velocity profiles, the only significant contribution to the total current comes from the region around the topmost cylinders. This demonstrates that streaming current measurements provide information only about the charge density in the outermost layer of the glycocalyx and may explain the discrepancy noted between electrokinetically and chemically determined charge density in the glycocalyx (Seaman 1983). Figure 7 also supports the assumption implicit in the model that the contribution of the charge on the plasma membrane of the cell can be neglected. Figure 8 shows the dependency of the streaming current on polymer concentration for three different salt concentrations. At, or above, physiological salt concentration the current is almost independent of salt concentration, but at one tenth physiological ionic strength the current is both higher and more sensitive to polymer concentration. The implication

is that electrokinetic experiments designed to determine the charge structure of the glycocalyx could be performed most effectively at low ionic strength.

As we showed above, flow through the glycocalyx appears at a distance as flow over a virtual plane at $x = x^*$. The streaming current density $j^*(x)$ generated by flow over this plane carrying a charge density q^* is:

$$j^*(x) = \kappa\lambda q^*(x - x^*)e^{-\kappa(x-x^*)} \qquad \text{and} \quad J^* = \int_{x^*}^{\infty} j^*\, dx = \frac{\lambda q^*}{\kappa}\ . \tag{3.5}$$

The current distribution above such a plate for a suitably chosen q^* is included in Figure 7. It will be seen that because the velocity close to the plate is lower than at a similar distance above the array of cylinders the maximum current density occurs further from the surface of the plate than the cylinders.

The currents due to the ion flux are very small, and are most easily detectable because of the streaming potential they induce. Assuming insulating boundary conditions, charge conservation requires a return conduction current on average equal and opposite to the streaming current. This return current is distributed over the entire vessel and not just the relatively thin glycocalyx layer. Associated with this current is the streaming potential, which is in practice measured as the difference, $\Delta\Phi$, between two electrodes inserted in the vessel. This measured value is therefore proportional to the electrode separation, to the wall shear-rate λ and to the vessel perimeter divided by its cross-sectional area. However, for Poiseuille flow in a cylindrical vessel, the pressure drop between the electrodes, Δp, is also proportional to these quantities and is easily measurable. The ratio $\Delta\Phi/\Delta p$ is therefore independent of vessel size and flow rate and is suitable for comparison between different experiments. The measurements are difficult to perform *in vivo*. Higher shear-rates and more controllable conditions are obtainable *in vitro*, but still the experimental conditions are not always specified fully in the literature. It should be noted that because of the relatively high conductivity and cross-sectional area of the blood vessels, the absolute magnitude of the streaming potential is smaller than the local potential due to ionic variations. There is thus little difference whether 'open circuit' or 'closed circuit' boundary conditions are imposed. This may not be the case for flows through the extracellular matrix, for example, where the currents flow through the same cross-sectional area.

At body temperature and ionic strength and a polymer concentration of 10% v/v, the model predicts a value

$$\frac{\Delta\Phi}{\Delta p} = \frac{1.3 \times 10^{-11}}{c\mu} = 8.6 \times 10^{-9}\ \text{V/Pa}\ , \tag{3.6}$$

assuming an electrical conductivity $c = 1.5\ \text{m}^{-1}\text{ohm}^{-1}$ and a viscosity $\mu = 10^{-3}$ Pa s. Macroscopic blood viscosity is four times larger, but on length-scales smaller than the red cells it is arguable that it is more appropriate to use the plasma viscosity in (3.6). In comparison, the *in vitro* measurements of Srinivasan *et al.* (1968) are $1.8{-}3.6\times10^{-9}$ V/Pa for canine carotid arteries. However, they also quote measurements *in vivo* of $0.2 - 0.5$ mV, a value orders of magnitude larger than predicted. Thubrikar *et al.* (1980) give an *in vivo* figure of 3.1×10^{-8} V/Pa, but seem to quote unrealistically large pressure drops across a canine femoral artery.

The above calculations are for axial flow whereas in the real system the polymer molecules may be orientated at random directions to the flow and some average of axial and transverse flows may be appropriate. In MMW we show that the streaming currents for axial and transverse flows are of similar magnitude but that, because of the higher resistance to flow in the transverse direction, the flow in the axial direction will be much

larger for a given pressure drop. There will also be a tendency for polymer chains to align with the flow. For flow in an isotropic medium, a weighting of one third axial to two thirds transverse has been proposed (Jackson & James 1986). In the two-dimensional system we envision a 50:50 split may be appropriate. In view of the non-linear dependence on the polymer concentration, the calculations should probably be performed at half the concentration for each condition, rather than averaging the results at full concentration. More extensive experimental data would be required to justified such an undertaking.

Electrophoretic Mobility

Figure 9 shows the flow across a line through the cylinder centres ($y = 0$) driven by a transverse electric field. The rods are stationary, so that the electrophoretic velocity is the constant value attained as $x \to \infty$. As x decreases down into the layers of cylinders, a periodic profile is soon reached, indicating that the electrophoretic mobility is independent of the depth of the layer.

Figure 10 shows the electrophoretic mobility for red blood cells with a glycocalyx of volume fraction 1% and a charge separation of 1.6 nm over the range of solution ionic strengths normally employed experimentally. Also shown in the figure are experimental data from Furchgott & Ponder (1941). The experimental data lie between the predicted mobilities for axial and transverse flows and an average between the two, as discussed in the previous section, would agree well. Also shown are the predictions of a one dimensional model from (Levine *et al.* 1983) with the parameters (glycocalyx thickness, 750 nm and polymer segment radius 70 nm) chosen best to fit the data. It should be noted, however, that our model requires the estimation of three parameters but that of Levine *et al.* requires an additional estimate of glycocalyx thickness. In the case of our model, the agreement with experiment could be improved at low salt concentrations by using the non-linear Poisson-Boltzmann equation.

Concluding remarks

We have demonstrated that a two-dimensional model of the glycocalyx can provide satisfactory agreement with experimental data both on streaming potentials in blood vessels and electrophoresis of red cells.

One of the most striking qualitative insights is the way in which the predictions depend only on the properties of the outermost layer of the glycocalyx and this is likely to be true, regardless of the details of the model, because of the effectively exponential decay of velocity into the layer. This has implications for the inference of properties of the glycocalyx from macroscopic measurements and for the analysis of cell-cell interactions. Above the layer, the potential decays exponentially while the velocity varies algebraically. It is thus plausible that changes in streaming potential would be the first detectable interaction as cells approach each other (Winlove & Parker 1987).

Some of the assumptions in our approach require consideration. We employed two widely used approximations, firstly that there is a uniform surface charge density on the cylinders representing the polymer chains and secondly that the cylinders are parallel and evenly spaced. We noted that any periodic charge variation down the rods merely re-defines the effective Debye length and does not alter the form of the solution nor dramatically alter our conclusions. It would be easy to include in the model variations in spacing of the rods, whether due to electrostatic repulsions or fluid shear (Damiano

1998). Flexibility of the polymer branches could best be addressed using scaling argument approaches, e.g. Harden *et al.* (1997).

Our modelling makes use of the linearised equations for the electrical potential, which is justified at physiological ionic strength but breaks down at the low ionic strength used in some experimental investigations of electrokinetic phenomena. Use of the full non-linear equation would be feasible but more cumbersome in most parameter ranges.

The limitations of the continuum based Poisson-Boltzmann approach have already been discussed in our earlier paper (MMW). The agreement with Monte-Carlo methods (e.g. Le Bret & Zimm 1984) is satisfactory even near molecular length-scales.

A. Mokady was supported by a prize studentship in Mathematical Biology awarded by the Wellcome Trust.

REFERENCES

Buschmann MD, Grodzinsky AJ. A molecular-model of proteoglycan-associated electrostatic forces in cartilage mechanics. Journal of Biomechanical Engineering 1995;117:179–192.

Chammas P, Federspiel WJ, Eisenberg SR. Microcontinuum model of electrokinetic coupling in the extracellular-matrix – perturbation formulation and solution. Journal of Colloid and Interface Science 1994;168:526-538.

Damiano ER. The effect of the endothelial-cell glycocalyx on the motion of red blood cells through capillaries. Microvascular research 1998;55:77–91.

Eisenberg SR, Grodzinsky AJ. Electrokinetic micromodel of extracellular-matrix and other polyelectrolyte networks. PhysicoChemical Hydrodynamics 1988;10:517–539.

Fixman M. The Poisson-Boltzmann equation and its application to polyelectrolytes. Journal of Chemical Physics 1979;70:4995–5005.

Furchgott RF, Ponder E. Electrophoretic studies on human red blood cells. Journal of General Physiology 1941;24:447–457.

Harden JL, Borisov OV, Cates ME. Deformation of polyelectrolyte brushes in strong flows: Good solvent regime. Macromolecules 1997;30:1179–1187.

Jackson GW, James DF. The permeability of fibrous porous media. Canadian Journal of Chemical Engineering 1986;64:364–374.

Katchalsky A. Polyelectrolytes. Pure and Applied Chemistry 1971;26:327–373.

Larson RE, Higdon JJL. Microscopic flow near the surface of two-dimensional porous media. Part 1. Axial Flow. Journal of Fluid Mechanics 1986;166:449–472.

Larson RE, Higdon JJL. Microscopic flow near the surface of two-dimensional porous media. Part 2. Transverse Flow. Journal of Fluid Mechanics 1987;178:119–136.

Le Bret M, Zimm BH. Monte-Carlo determination of the distribution of ions about a cylindrical polyelectrolyte. Biopolymers 1984;23:271–285.

Levine S, Levine M, Sharp KA, Brooks DE. Theory of the electrokinetic behaviour of human erythrocytes. Biophysical Journal 1983;42:127–135.

Mokady AJ, Mestel AJ, Winlove CP. Flow through a charged biopolymer layer. Journal of Fluid Mechanics 1999;383:353–378.

Seaman GVF. The electrochemical properties of the peripheral zone of erythrocytes. Annals of the New York Academy of Sciences 1983;416:176–189.

Srinivasan S, Aaron R, Chopra PS, Lucas T, Sawyer PN. Effect of thrombotic and antithrombotic drugs on the surface charge characteristics of canine blood vessels: In vivo and in vitro studies. Surgery 1968;64:827–833.

Thubrikar M, Reich T, Cadoff I. Study of surface charge of the intima and artificial materials in relation to thrombogenicity. Journal of Biomechanics 1980;13:663–666.

Weinbaum S. Models to solve mysteries in biomechanics at the cellular level; a new view of fiber matrix layers. Annals of Biomedical Engineering 1998;26:627–643.

Winlove CP, Parker KH. Electrokinetic effects on luminal and transmural fluid flow in capillaries. Biorheology 1987;24:783–793.

Figure captions

FIGURE 1: A semi-infinite, doubly periodic array of charged cylinders. Schematic representations of the potential (left) and shear driven axial flow (right) are drawn (i) midway between cylinders ($y = b$) and (ii) passing through the cylinders ($y = 0$). The potential decays exponentially with the Debye length in $x > 0$, and soon becomes periodic as $x \to -\infty$. The velocity becomes self-similar in $x < 0$, decaying with a scale factor from cylinder to cylinder.

FIGURE 2: The mean non-dimensional potential, $\phi = e\Phi/(kT)$, over the boundary of a square domain as a function of polymer concentration for three electrolyte molarities.

FIGURE 3a: The nondimensional potential $\phi = e\Phi/(kT)$, as a function of radius, plotted for $\theta = 0$ (top curve) and $\theta = \frac{1}{4}\pi$ (bottom curve.) The middle curve is the cylindrical cell approximation. The polymer concentration is 10% v/v in a 0.15 M monovalent electrolyte, so that $b = 2.80a$, $b_0 = 3.16a$, $b\sqrt{2} = 3.96a$ while $\kappa^{-1} = 1.6a$.

FIGURE 3b: The variation of the mean potential over the outer domain boundary with polymer concentration for a 0.15 M electrolyte. The line-charge and cylindrical cell approximations are also shown.

FIGURE 4: Comparison of the linear and non-linear Poisson-Boltzmann equations using a cylindrical cell approximation. The value of ϕ at the outer cylindrical cell boundary is plotted against the concentration of the surrounding electrolyte solution. The polymer concentration is 1% v/v in figure (a) and 10% in figure (b).

FIGURE 5: The potential ϕ for a semi-infinite square array of cylinders calculated at the centreline $y = 0$ and between the cylinders $y = b$. The polymer concentration is 10% v/v in (a) and 1% in (b) in both cases for a 0.015 M electrolyte. The line charge approximations are also shown.

FIGURE 6: The predicted monovalent ion concentrations for a 0.15 M electrolyte and a 10% polymer concentration. The results are for a temperature of 277 K and a charge separation of 1.4 nm.

FIGURE 7: The local non-dimensional axial current density $j(x, 0)$ and $j(x, b)$ for a semi-infinite array of cylinders and for an equivalent charged flat plate $j^*(x)$ (see text $x^* = -1.802a$, $q^* = 0.487\varepsilon qa$) for unit shear ($\lambda = 1$), a 10% polymer concentration and a 0.15 M monovalent electrolyte.

FIGURE 8: Variation with polymer concentration of the non-dimensional axial streaming current, J, for different electrolyte molarities. The calculation is for a temperature of 277 K, and a charge spacing of 1.4 nm.

FIGURE 9: The velocity profile for a transverse electric field, plotted along $y = 0$ with the cylinders stationary. The electrophoretic velocity is given by the value as $x \to \infty$. A few cylinders down from the surface, the flow is almost periodic.

FIGURE 10: The variation of electrophoretic mobility with molarity for a 1% polymer concentration. Experimental data from Furchgott & Ponder (1941) are compared with our predictions for axial and transverse flows and lie between the axial and transverse curves. Also shown is an optimally-fitted one-dimensional model from Levine et al. (1983). The temperature is 298 K and the charge separation is 1.6 nm. The mobility is in units of 10^{-8} $m^2/(Vs)$.

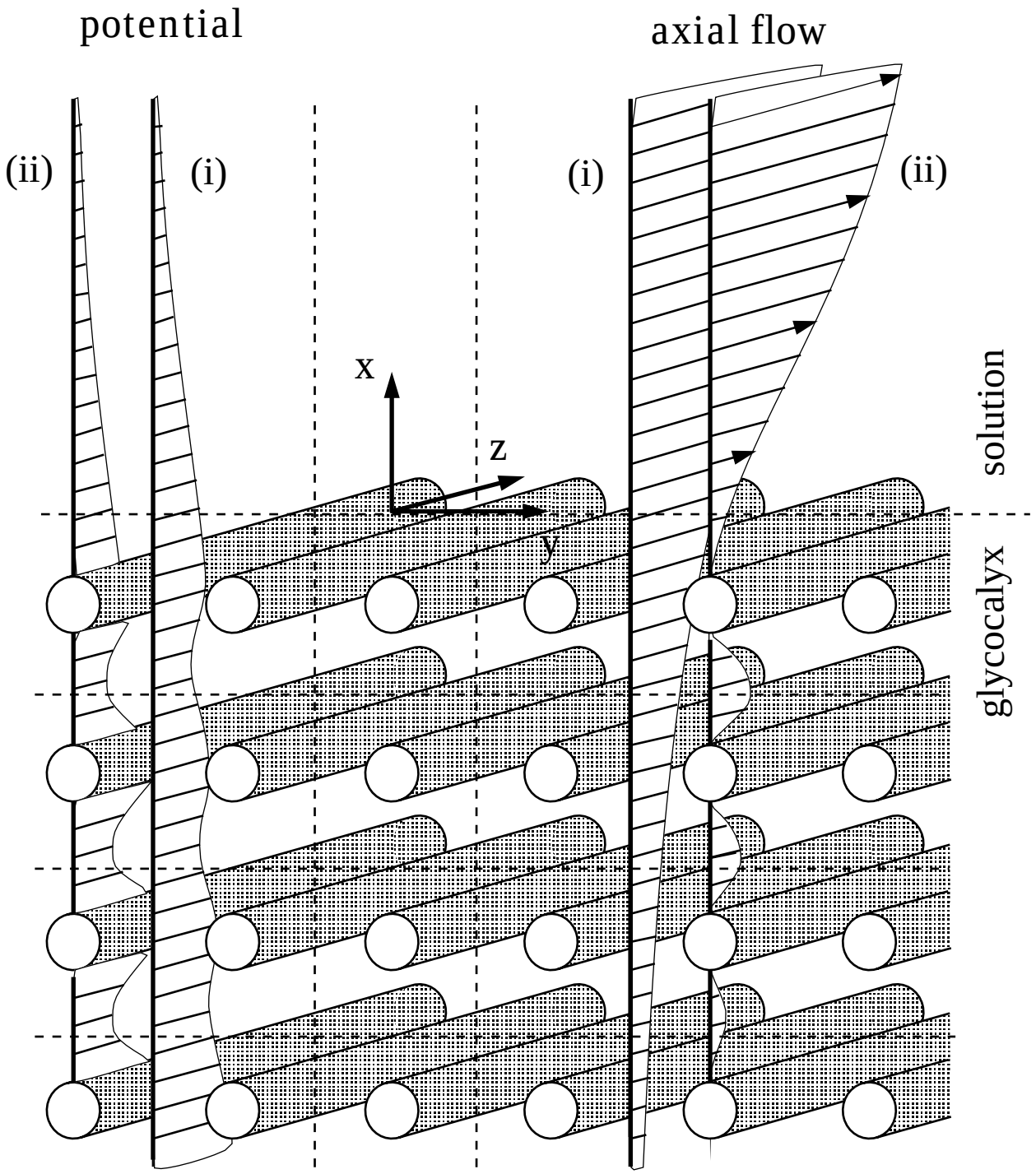
potential
axial flow
(ii)
(i)
(i)
(ii)
x
z
y
solution
glycocalyx

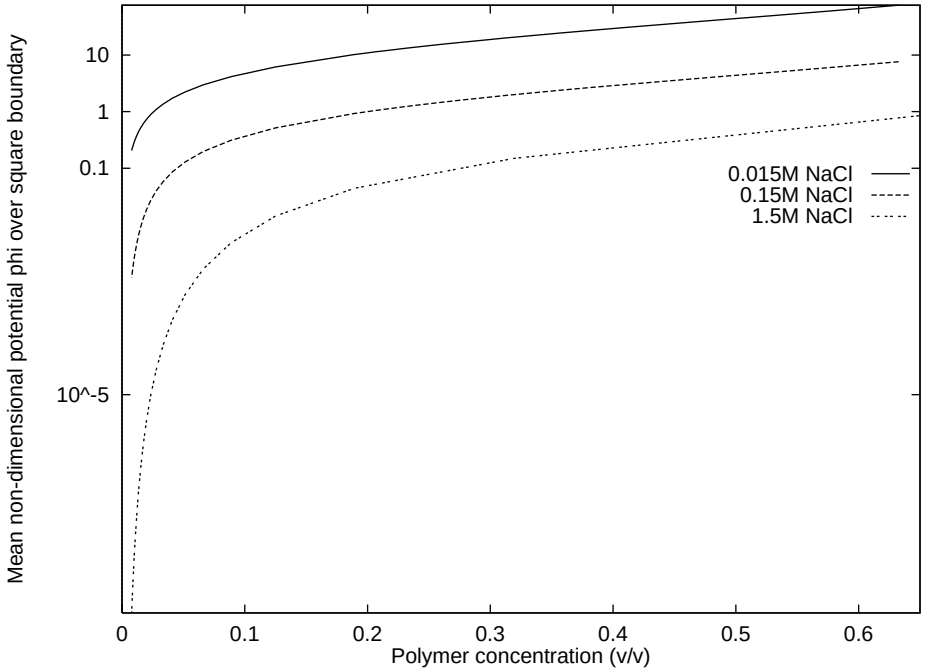
Mean non-dimensional potential phi over square boundary
10
1
0.1
10^-5
0.015M NaCl
0.15M NaCl
1.5M NaCl
0
0.1
0.2
0.3
0.4
0.5
0.6
Polymer concentration (v/v)

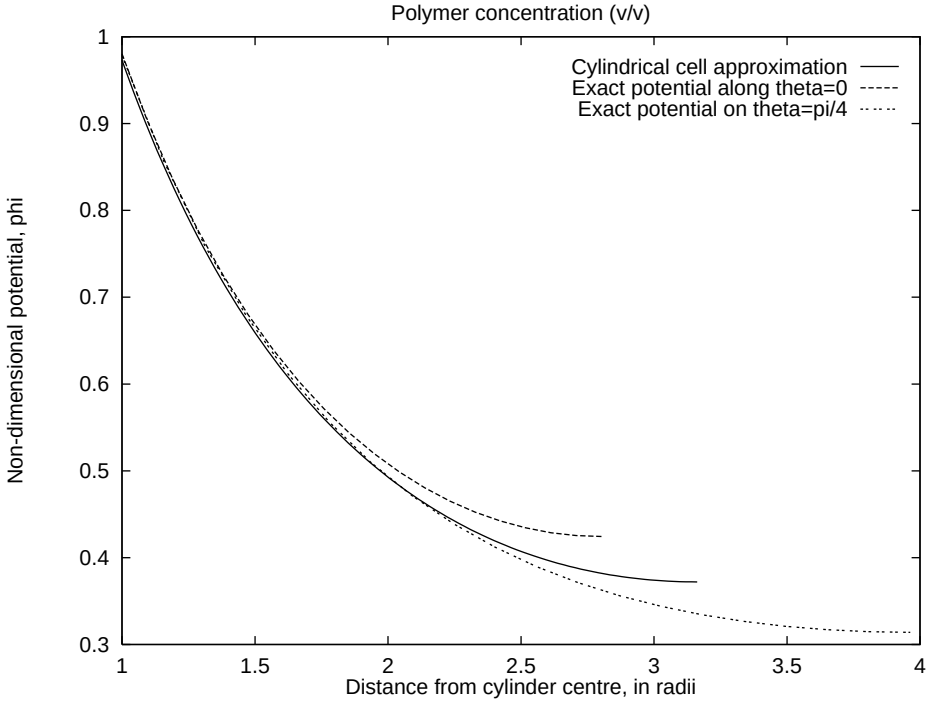
Non-dimensional potential, phi
1
0.9
0.8
0.7
0.6
0.5
0.4
0.3
Cylindrical cell approximation
Exact potential along theta=0
Exact potential on theta=pi/4
1
1.5
2
2.5
3
3.5
4
Distance from cylinder centre, in radii

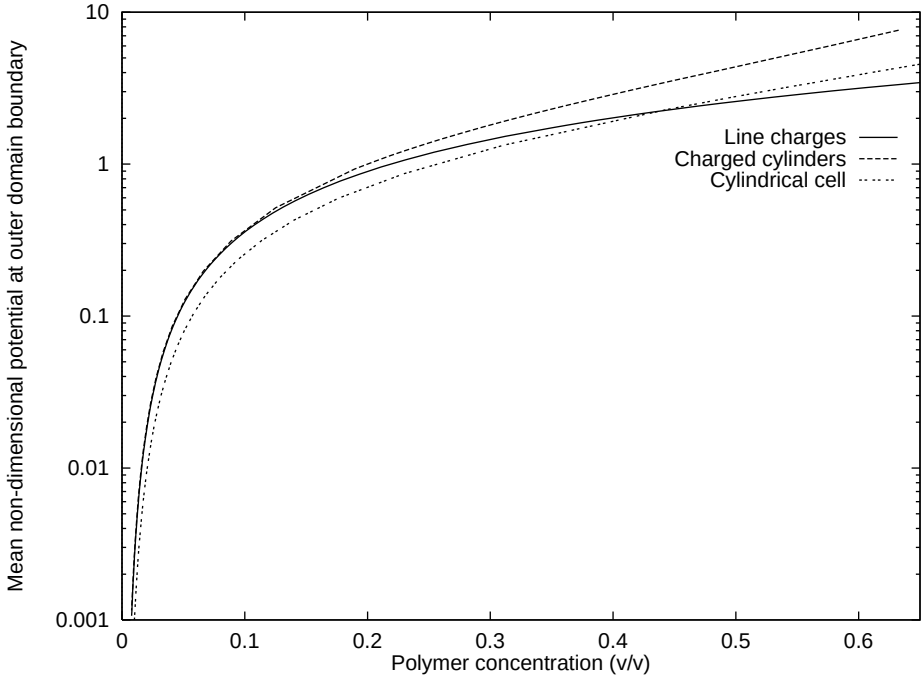
Mean non-dimensional potential at outer domain boundary
10
1
0.1
0.01
0.001
0
0.1
0.2
0.3
0.4
0.5
0.6
Polymer concentration (v/v)
Line charges
Charged cylinders
Cylindrical cell

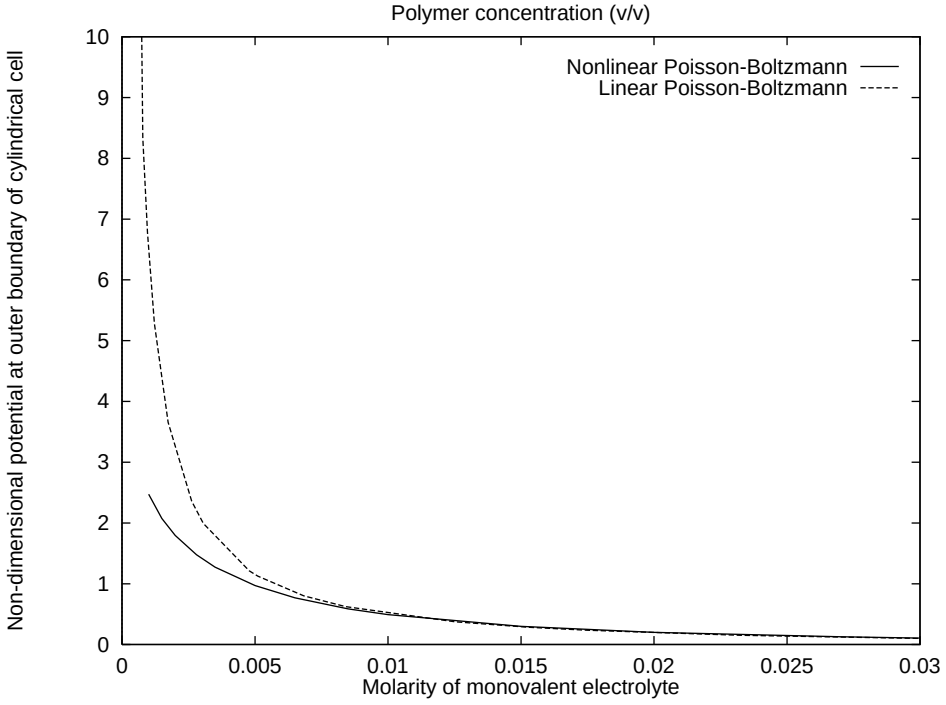
Non-dimensional potential at outer boundary of cylindrical cell
10
9
8
7
6
5
4
3
2
1
0
0
0.005
0.01
0.015
0.02
0.025
0.03
Molarity of monovalent electrolyte
Nonlinear Poisson-Boltzmann
Linear Poisson-Boltzmann

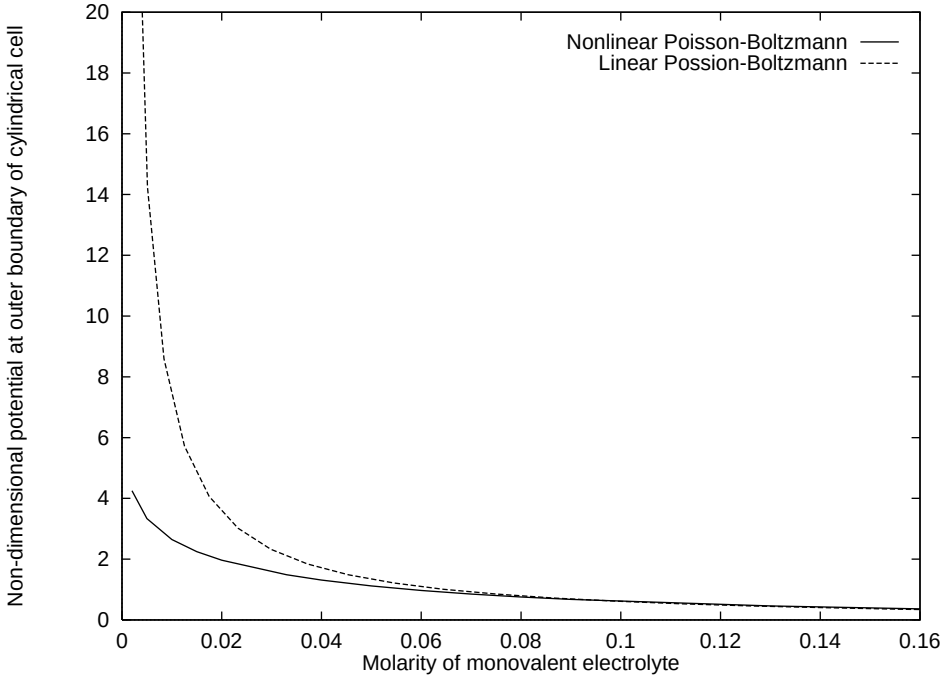
Non-dimensional potential at outer boundary of cylindrical cell
Molarity of monovalent electrolyte
Nonlinear Poisson-Boltzmann
Linear Possion-Boltzmann
0
2
4
6
8
10
12
14
16
18
20
0
0.02
0.04
0.06
0.08
0.1
0.12
0.14
0.16

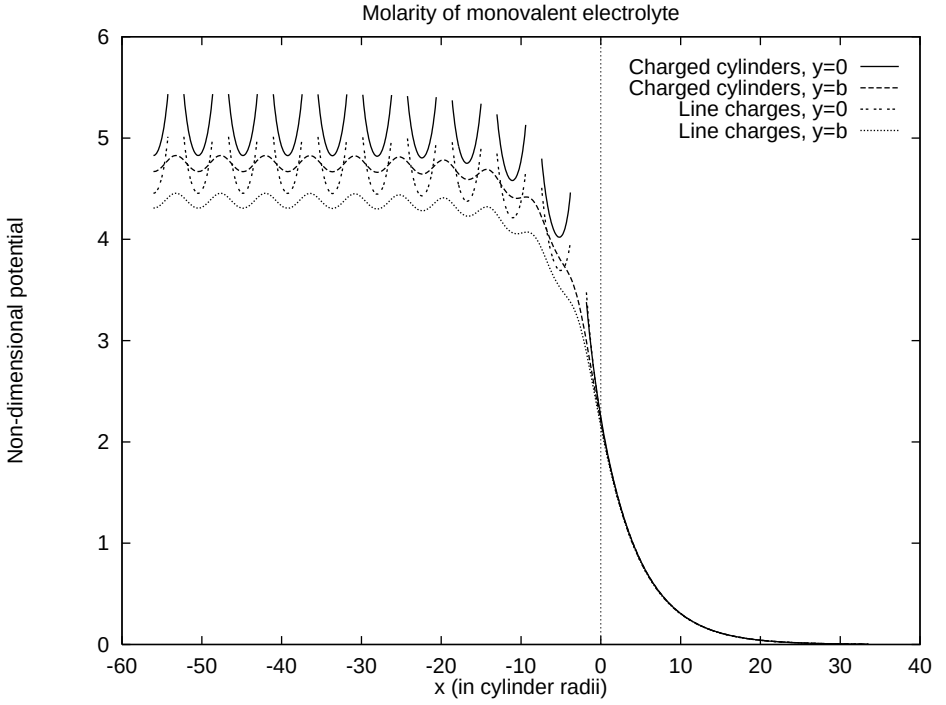
Non-dimensional potential
x (in cylinder radii)
Charged cylinders, y=0
Charged cylinders, y=b
Line charges, y=0
Line charges, y=b
0
1
2
3
4
5
6
-60
-50
-40
-30
-20
-10
0
10
20
30
40

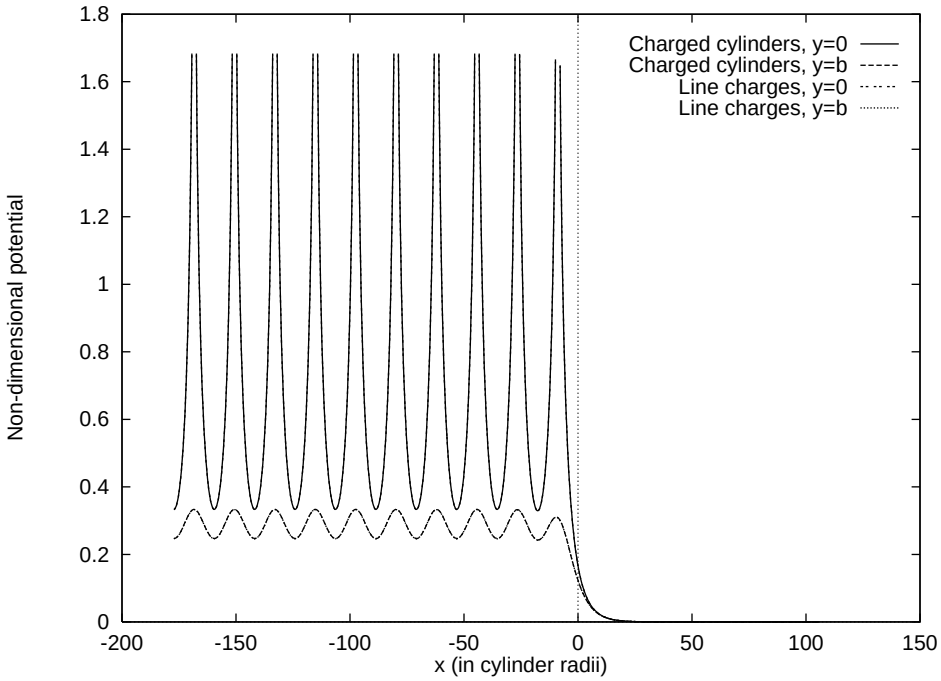
Charged cylinders, y=0
Charged cylinders, y=b
Line charges, y=0
Line charges, y=b
Non-dimensional potential
x (in cylinder radii)
1.8
1.6
1.4
1.2
1
0.8
0.6
0.4
0.2
0
-200
-150
-100
-50
0
50
100
150

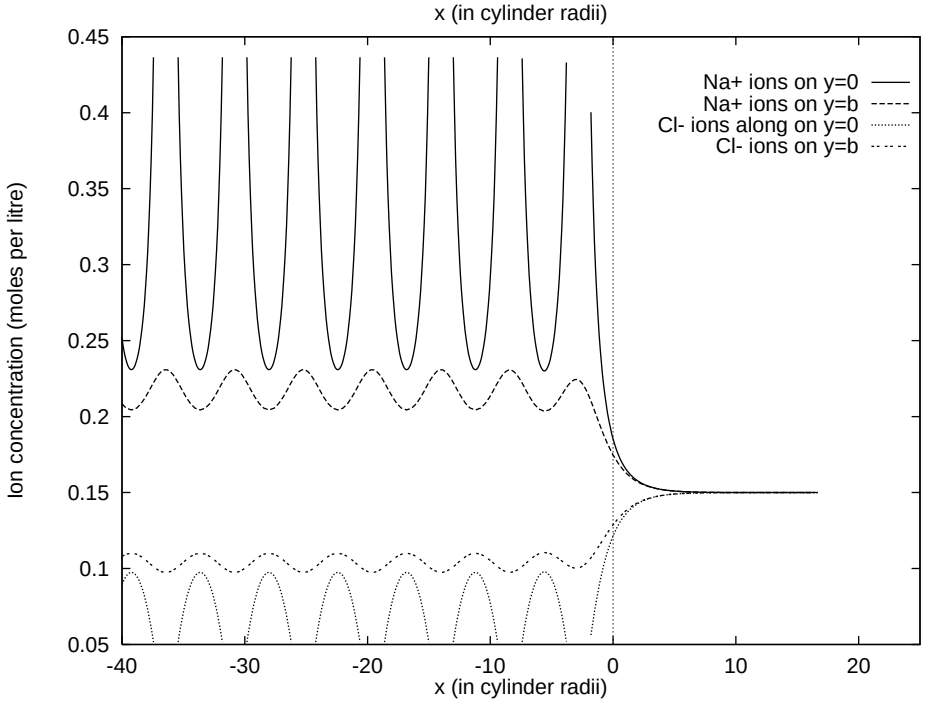
Na+ ions on y=0
Na+ ions on y=b
Cl- ions along on y=0
Cl- ions on y=b
Ion concentration (moles per litre)
x (in cylinder radii)
0.45
0.4
0.35
0.3
0.25
0.2
0.15
0.1
0.05
-40
-30
-20
-10
0
10
20

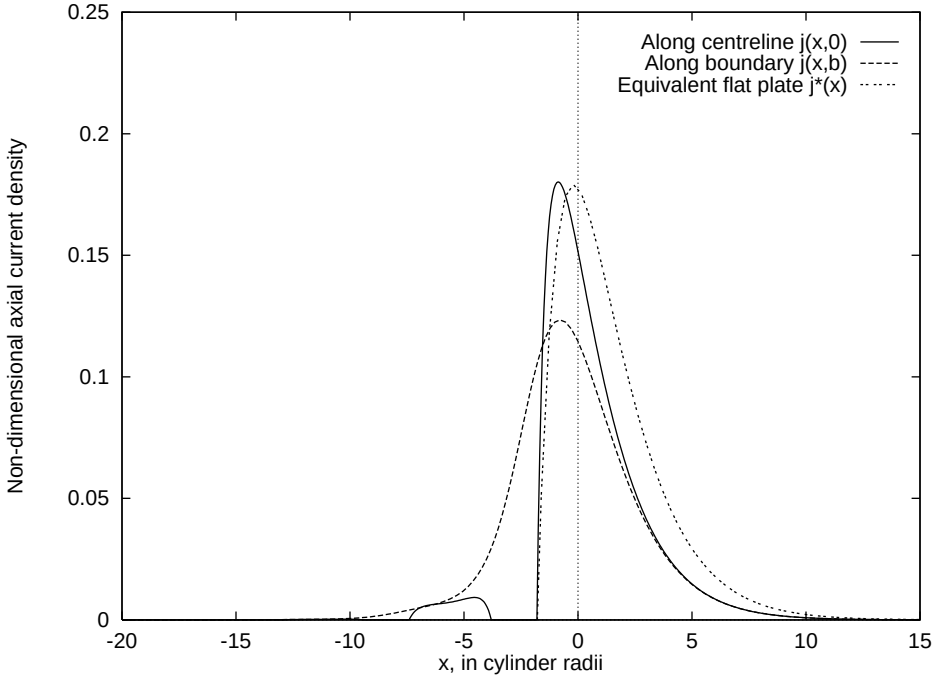
Along centreline j(x,0)
Along boundary j(x,b)
Equivalent flat plate j*(x)
Non-dimensional axial current density
x, in cylinder radii
0.25
0.2
0.15
0.1
0.05
0
-20
-15
-10
-5
0
5
10
15

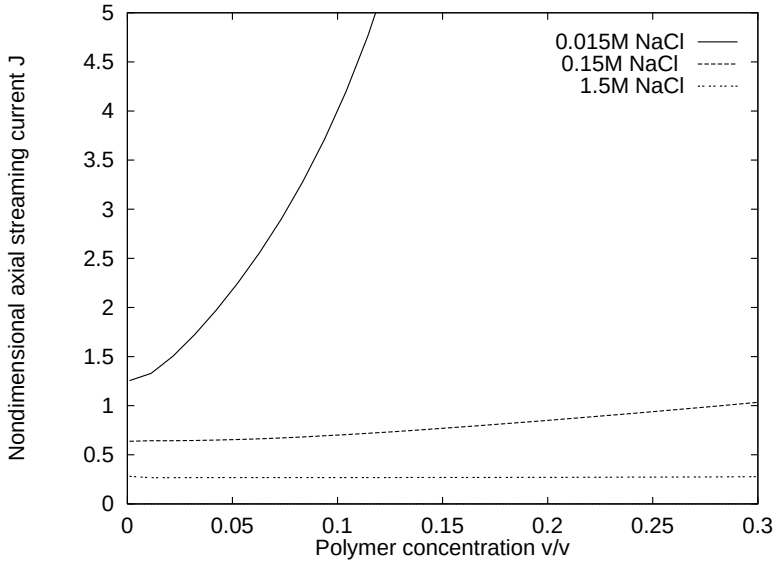
0.015M NaCl
0.15M NaCl
1.5M NaCl
Nondimensional axial streaming current J
Polymer concentration v/v
5
4.5
4
3.5
3
2.5
2
1.5
1
0.5
0
0
0.05
0.1
0.15
0.2
0.25
0.3

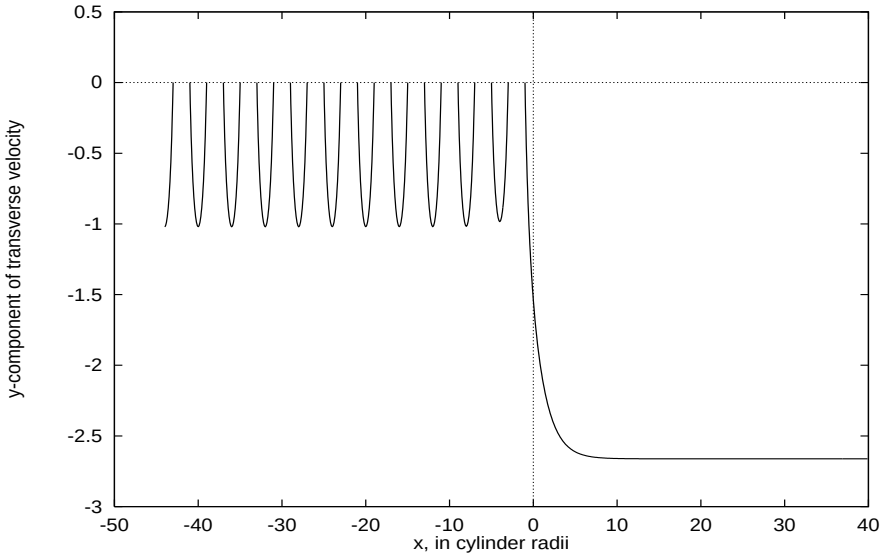
y-component of transverse velocity
x, in cylinder radii
0.5
0
-0.5
-1
-1.5
-2
-2.5
-3
-50
-40
-30
-20
-10
0
10
20
30
40

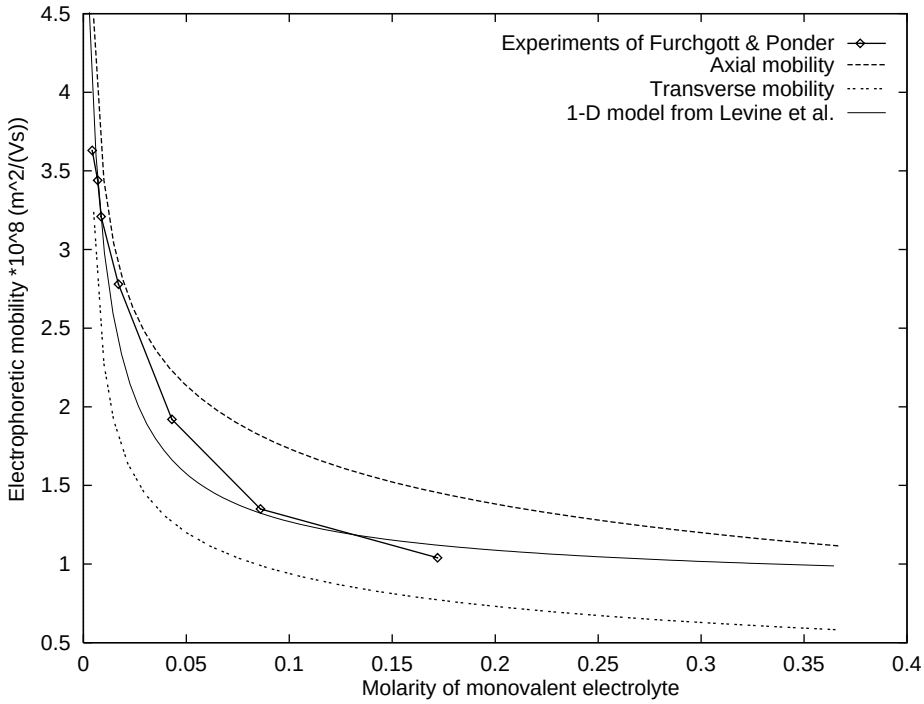
Experiments of Furchgott & Ponder
Axial mobility
Transverse mobility
1-D model from Levine et al.
Electrophoretic mobility *10^8 (m^2/(Vs))
Molarity of monovalent electrolyte
4.5
4
3.5
3
2.5
2
1.5
1
0.5
0
0.05
0.1
0.15
0.2
0.25
0.3
0.35
0.4